Full-field refractive index distribution measurement of a gradient-index lens with heterodyne interferometry

2010 Meas. Sci. Technol. 21 105310

(http://iopscience.iop.org/0957-0233/21/10/105310)

Meas. Sci. Technol. **21** (2010) 105310 (5pp) doi:10.1088/0957-0233/21/10/105310

Full-field refractive index distribution measurement of a gradient-index lens with heterodyne interferometry

Hung-Chih Hsieh, Yen-Liang Chen, Wang-Tsung Wu, Wei-Yao Chang and Der-Chin Su[1]

Department of Photonics and Institute of Electro-Optical Engineering, National Chiao-Tung University, 1001 Ta-Hsueh Road, Hsinchu 30050, Taiwan, Republic of China

E-mail: t7503@faculty.nctu.edu.tw

Received 8 March 2010, in final form 19 August 2010
Published 14 September 2010
Online at stacks.iop.org/MST/21/105310

Abstract
A light beam coming from a circular heterodyne light source with an electro-optic modulator is incident on a gradient-index lens obliquely. The reflected light passes through an analyzer and an imaging lens, and is recorded by a fast CMOS camera. A group of periodic sinusoidal segments recorded by each pixel is modified, and its associated phase is derived with a unique technique. The processes are applied to other pixels; the two-dimensional phase distribution can be obtained similarly. The estimated data are substituted into the special equations derived from Fresnel's equations, and the full-field refractive index distribution of the gradient-index lens can be obtained. This method has the merits of both common-path interferometry and heterodyne interferometry.

Keywords: GRIN lens, heterodyne interferometry, full-field measurement, refractive index, sine wave fitting algorithm

(Some figures in this article are in colour only in the electronic version)

1. Introduction

Gradient-index (GRIN) lenses [1–3] and GRIN devices are finding an increasing role in applications as diverse as telecommunications, medicine, and industrial and biomedical sensing [4, 5]. Knowledge of the refractive index of the GRIN lens is important not only to assess its performance in optical devices, but also to control the quality of products. Several non-destructive and non-contact optical methods [6–13] have been proposed and they have good measurement results. Dragomir *et al* [6, 7] used the quantitative phase microscopy (QPM) technique to measure the 3D refractive index distribution of a GRIN lens, and the resolution can be reduced to 10^{-4}. The QPM technique can have good experimental results; however, the sample must be immersed in a medium of refractive index that matches the surface index of the tested GRIN lens. This means that the surface refractive index of the GRIN lens must be either accurately known or assumed [12]. Besides, the QPM technique can measure the 3D refractive index distribution, but the tested sample needs to be rotated. This makes the experiment more complicated and more time consuming. In this paper, we proposed an accurate and time-saving method for measuring the full-field refractive index distribution of the GRIN lens. In this method, light coming from a circular heterodyne light source is incident on the GRIN lens obliquely. The reflected light passes through an analyzer and an imaging lens. The full-field interference signals produced by the components of the s- and the p-polarized light are recorded by a fast CMOS camera. By using Chen's technique [14], each pixel records a group of periodic sinusoidal segments, whose phase is related to the refractive index of the GRIN lens. Next, let its period be so lengthened that the periodic sinusoidal segments become a continuous sinusoidal signal. Based on a least-squares sine-wave-fitting algorithm [14–16], an optimal fitted sine wave curve and the associated phase can be obtained. If these processes are applied to other pixels, then their phases can

[1] Author to whom any correspondence should be addressed.

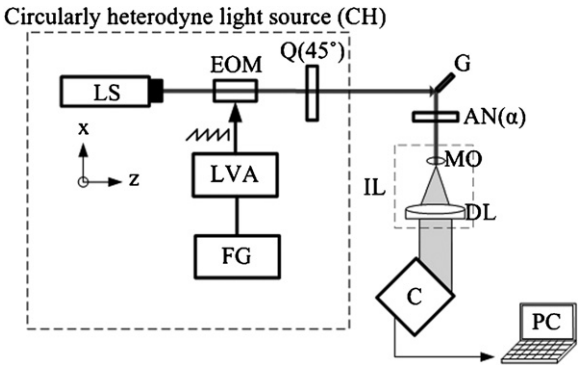

Figure 1. The optical configuration of this method. LS: light source; EOM: electro-optic modulator; FG: function generator; LVA: linear voltage amplifier; Q: quarter-wave plate; G: GRIN lens; AN: analyzer; IL: imaging lens; MO: microscopic objective; DL: doublet; C: CMOS camera.

be obtained similarly. Finally, the full-field phase distribution can be calculated. Consequently, the estimated data are substituted into the special equations derived from Fresnel's equations [17], and the full-field refractive index distribution of the GRIN lens can be obtained. For the purpose of easy observation, a color map is used to represent the resultant refractive index distribution. The validity of this method is proved. It has merits of both common-path interferemetry [18] and heterodyne interferemetry [19, 20], that is high stability, simple configuration, easy operation, time saving and high resolution.

2. Principle

2.1. The phase of the interference signal

The optical configuration of this method is shown in figure 1. For convenience, the z-axis is chosen along the light propagation direction and the y-axis is along the vertical direction. The circular heterodyne light source (CH) [19–21] is composed of a light source (LS), an electro-optic modulator (EOM), a function generator (FG) and a linear voltage amplifier (LVA). The Jones vector of the light beam coming from the CH can be written as [19–21]

$$E_{\mathrm{CH}} = \frac{1}{2}\begin{pmatrix}1\\ \mathrm{i}\end{pmatrix}\mathrm{e}^{\mathrm{i}\pi ft}\,\mathrm{e}^{\mathrm{i}2\pi f_0 t} + \frac{1}{2}\begin{pmatrix}\mathrm{i}\\ 1\end{pmatrix}\mathrm{e}^{-\mathrm{i}\pi ft}\,\mathrm{e}^{\mathrm{i}2\pi f_0 t}, \qquad (1)$$

where f_0 is the light frequency and f is the frequency difference between the right- and the left-circular polarizations. It is incident at 45° on the tested GRIN lens (G) with the refractive index distribution $n(x, y)$. The reflected light beam passes through an analyzer (AN) with the transmission axis at 45° to the x-axis and an imaging lens (IL). The IL is used to image the surface of the G onto the image plane of the CMOS camera (C). Consequently, the Jones vector of the light at the C becomes

$$\begin{aligned} E_C &= \boldsymbol{AN}(45^\circ)\boldsymbol{G}E \\ &= \begin{pmatrix}\cos^2 45^\circ & \sin 45^\circ\cos 45^\circ\\ \sin 45^\circ\cos 45^\circ & \sin^2 45^\circ\end{pmatrix} \\ &\quad\times\begin{pmatrix}r_p & 0\\ 0 & r_s\end{pmatrix}\frac{1}{2}\begin{pmatrix}\mathrm{e}^{\mathrm{i}\pi ft}+\mathrm{i}\,\mathrm{e}^{-\mathrm{i}\pi ft}\\ \mathrm{i}\,\mathrm{e}^{\mathrm{i}\pi ft}+\mathrm{e}^{-\mathrm{i}\pi ft}\end{pmatrix}\mathrm{e}^{\mathrm{i}2\pi f_0 t} \\ &= \frac{1}{4}\begin{pmatrix}r_p(\mathrm{e}^{\mathrm{i}\pi ft}+\mathrm{i}\,\mathrm{e}^{-\mathrm{i}\pi ft})+r_s(\mathrm{i}\,\mathrm{e}^{\mathrm{i}\pi ft}+\mathrm{e}^{-\mathrm{i}\pi ft})\\ r_p(\mathrm{e}^{\mathrm{i}\pi ft}+\mathrm{i}\,\mathrm{e}^{-\mathrm{i}\pi ft})+r_s(\mathrm{i}\,\mathrm{e}^{\mathrm{i}\pi ft}+\mathrm{e}^{-\mathrm{i}\pi ft})\end{pmatrix}\mathrm{e}^{\mathrm{i}2\pi f_0 t}, \end{aligned} \qquad (2)$$

where $\boldsymbol{AN}$ and $\boldsymbol{G}$ are the Jones matrices of the AN and the G, respectively. r_s and r_p are the amplitude reflection coefficients of the G, and they can be written as

$$r_p = \frac{n\cos 45^\circ - \frac{\sqrt{n^2-\sin^2 45^\circ}}{n}}{n\cos 45^\circ + \frac{\sqrt{n^2-\sin^2 45^\circ}}{n}}, \qquad (3)$$

and

$$r_s = \frac{\cos 45^\circ - \sqrt{n^2-\sin^2 45^\circ}}{\cos 45^\circ + \sqrt{n^2-\sin^2 45^\circ}}. \qquad (4)$$

Hence, the intensity of the interference signal recorded by the C is

$$\begin{aligned} I &= |E_{\mathrm{C}}|^2 \\ &= \frac{1}{16}\left|\begin{matrix}r_p(\mathrm{e}^{\mathrm{i}\pi ft}+\mathrm{i}\,\mathrm{e}^{-\mathrm{i}\pi ft})+r_s(\mathrm{i}\,\mathrm{e}^{\mathrm{i}\pi ft}+\mathrm{e}^{-\mathrm{i}\pi ft})\\ r_p(\mathrm{e}^{\mathrm{i}\pi ft}+\mathrm{i}\,\mathrm{e}^{-\mathrm{i}\pi ft})+r_s(\mathrm{i}\,\mathrm{e}^{\mathrm{i}\pi ft}+\mathrm{e}^{-\mathrm{i}\pi ft})\end{matrix}\right|^2 \\ &= \frac{r_p^2+r_s^2}{4}+\frac{1}{4}\left[\left(r_p^2-r_s^2\right)\sin(2\pi ft)+2r_p r_s\cos(2\pi ft)\right] \\ &= I_0(1+\gamma\cos(2\pi ft+\phi)), \end{aligned} \qquad (5)$$

where $I_0 = \frac{1}{4}\left(r_p^2+r_s^2\right)$, $\gamma = 1/I_0$. ϕ is the phase of the interference signal; it can be written as

$$\phi(x, y) = \tan^{-1}\left(\frac{n^2-1}{\sqrt{2n^2-1}}\right). \qquad (6)$$

Equation (6) can be rewritten as

$$n(x, y) = \begin{cases}\sqrt{\sec^2\phi+\sec\phi\tan\phi}, & \text{if} \quad 0 \leqslant \phi < \frac{\pi}{2}\\ \sqrt{\sec^2\phi-\sec\phi\tan\phi}, & \text{if} \quad -\frac{\pi}{2} < \phi < 0.\end{cases} \qquad (7)$$

It is obvious from equation (7) that $n(x, y)$ can be calculated from the measurement of $\phi(x, y)$.

2.2. Phase estimation with heterodyne interferometry

The EOM with a half-wave voltage V_π in the CH is driven by an external sawtooth voltage signal with a frequency f and an amplitude V. The C with a frame frequency f_s and a frame exposure time Δt is used to take s frames in the measurement time T. Because there is no reference signal for evaluating the phase as in conventional heterodyne interferometry, we use Chen's technique [14] and let V be smaller than V_π. Consequently, each pixel records a group of periodic sinusoidal segments with a period τ and each segment has an initial phase ψ, as shown in figure 2. Here, we have

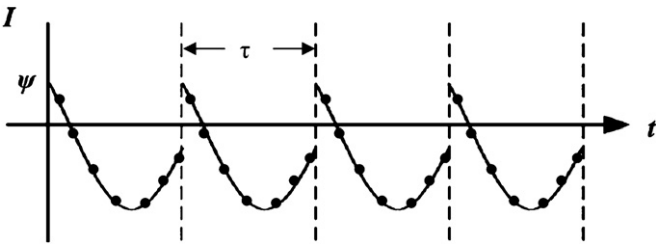

Figure 2. The sampled interference signals as $V < V_\pi$.

$\psi = \phi - \phi_0$, and $\phi_0 = \pi V / V_\pi$ is the characteristic phase. Next, let the period τ be lengthened to $\tau + (V_\pi - V)/Vf$ as Chen did, then the interference signal can be modified to a continuous sinusoidal signal and represented as

$$I_c(t_k) = I_0 \left(1 + \gamma \cos\left(2\pi \frac{V}{V_\pi \tau} t_k + \psi\right)\right). \tag{8}$$

Then, equation (8) is processed by using the three-parameter sine-wave-fitting algorithm [15, 16] to get the phase data ψ, and the fitted equation has the form of

$$\begin{aligned} I'(t_k) &= A_0 \cos(2\pi f t_k) + B_0 \sin(2\pi f t_k) + C_0 \\ &= \sqrt{A_0^2 + B_0^2} \cos(2\pi f t_k + \psi), \end{aligned} \tag{9}$$

where

$$\psi = \tan^{-1}\left(-\frac{B_0}{A_0}\right), \tag{10}$$

where A_0, B_0 and C_0 are real numbers, and they can be derived with the least-squares method [15]. Consequently, the phase ϕ can be obtained by calculating $\phi = \psi + \phi_0$ under the condition that V and V_π are specified. If these processes are applied to other pixels, then their phases can be obtained similarly. Finally, the full-field phase distribution $\phi(x, y)$ can be obtained.

3. Experiments and results

In order to show the feasibility of this method, a GRIN lens (AC Photonics, Inc./ALC-18) with a NA of 0.46, a diameter of 1.8 mm and a length of 0.25 pitch is tested. An He–Ne laser source with a wavelength λ of 632.8 nm is used as a light source. The EOM (New Focus/Model 4002) with a half-wave voltage of 148 V is driven by a 30 Hz sawtooth wave with a peak-to-peak voltage of 120 V. The magnification of the IL is −4. A CMOS camera (Baslar/A504K) with 256 gray levels and 600 × 600 pixels is used and its dimension is 12 μm × 12 μm. It is used under the conditions $f = 30$ Hz, $f_s = 450$ Hz, $\Delta t = 10^{-3}$ s and $T = 1$ s. The interferograms are sent to a personal computer, and they are analyzed and calculated with the software Matlab (MathWorks Inc.). For easier reading, $n(x, y)$ is displayed in color as shown in figure 3 and the associated refractive index contour is also depicted in figure 4.

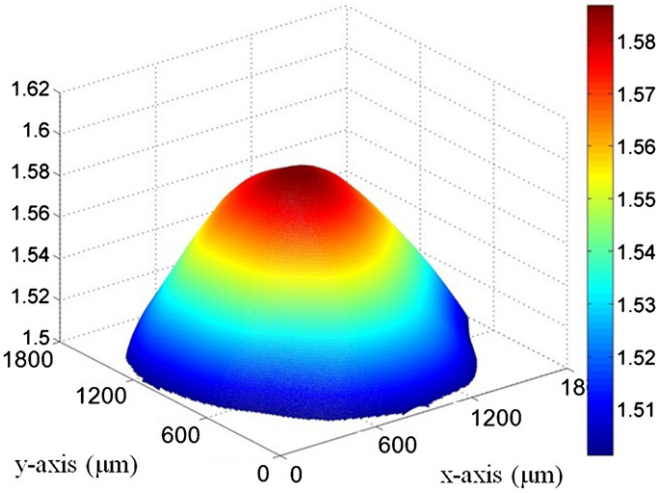

Figure 3. Two-dimensional refractive index distribution of the GRIN lens for $\lambda = 632.8$ nm.

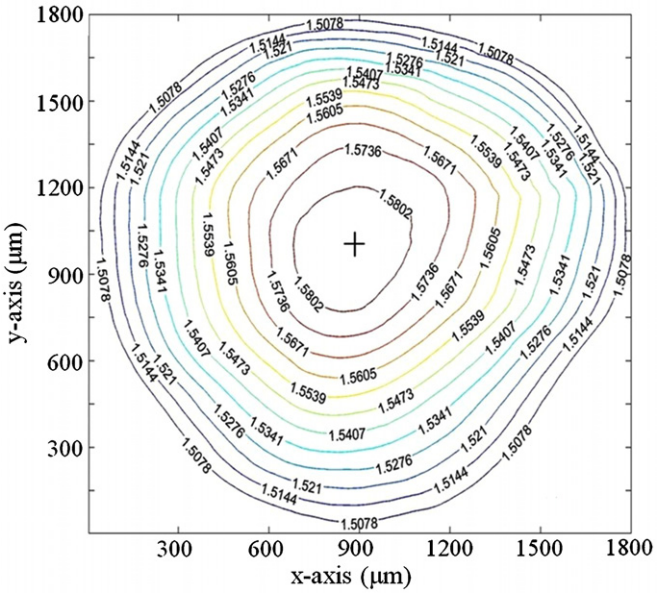

Figure 4. Refractive index contour of the GRIN lens for $\lambda = 632.8$ nm.

4. Discussion

From equation (7), we have

$$\Delta n = \left|\frac{\partial n}{\partial \theta}\right| \Delta\theta + \left|\frac{\partial n}{\partial \phi}\right| \Delta\phi, \tag{11}$$

where Δn, $\Delta\theta$ and $\Delta\phi$ are the errors of n, the incident angle θ and ϕ, respectively, the error $\Delta\theta$ coming from the misalignment of the incident angle. In our experiment, it relates to the resolution of the rotation stage (SIGMA/SGSP-160YAW), and is about 0.01°. Next, the error $\Delta\phi$ may be caused by the sampling error $\delta\phi_1$ [22], the polarization mixing error $\delta\phi_2$ [23, 24] and the characteristic phase error $\delta\phi_3$ [25]. Because an area scan digital camera is used to record the full-field heterodyne interference signals, the measurement resolution depends on the parameters f_s, T and g. Although $\delta\phi_1$ becomes smaller as T, g and f_s/f increase, the data processing also becomes time consuming. In theory, Tf is an integer and larger than 1, the same frame data are recorded repeatedly Tf times and $\delta\phi_1$ hardly becomes smaller. To decrease the effect coming from the instability of frequency difference f and minimize the phase error, we choose the conditions $f_s/f = 15$ and $T = 1$ s as suggested by Jian [18]. Consequently, $\delta\phi_1$ can be minimized to 0.036°. Owing to the extinction ratio effect of a polarizer, the mixing of light polarizations occurs. $\delta\phi_2$ can be reduced to 0.027° [19, 20] as the extinction ratio of the AN (Newport Inc.) is 1×10^{-3}. The errors in V and V_π directly introduce a systematic error $\delta\phi_3$. The resolution of V from the FG is $\Delta V_1 = 0.016$ V. V_π can also be measured [25], and its error is estimated to be $\Delta V_2 = 0.015$ V. Hence the

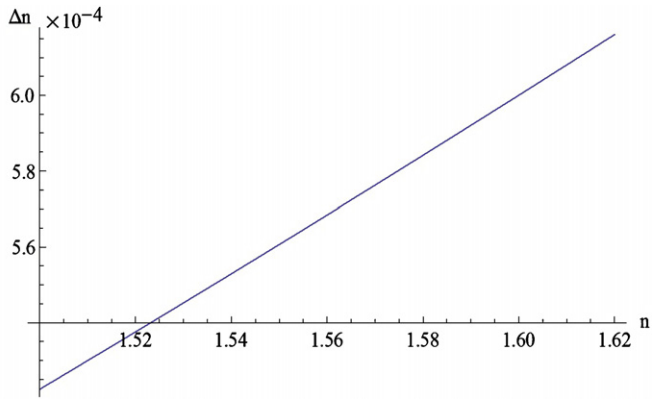

Figure 5. Relation curve of Δn versus n.

maximum error of $\delta\phi_3$ can be estimated and expressed as $\delta\phi_3 = \phi_{\max} \cdot [(\Delta V_1/V)^2 + (\Delta V_2/V)^2]^{1/2} \approx 0.03^\circ$, where $\phi_{\max} = 180^\circ$ is the maximum possible phase. In addition, the effect of surrounding vibration and air turbulence on the phase measurement error can be negligible due to the common-path optical configuration [26]. So, the total experimental phase error is $\Delta\phi = \delta\phi_1 + \delta\phi_2 + \delta\phi_3 \approx 0.093^\circ$. Consequently, substituting $\Delta\theta = 0.01^\circ$ and $\Delta\phi = 0.093^\circ$ into equation (11), the relation curve of Δn versus n can be calculated and is depicted in figure 5. It can be seen that Δn can be reduced to 6×10^{-4} as $n = 1.6$.

To collect the reflected parallel beam from the GRIN lens and magnify the object simultaneously, it is better to use IL composed of a microscopic objective (MO) and a doublet (DL). The transverse magnification of IL in our experiments is -4. Because the IL is an afocal optical system, the GRIN lens needs to be located in the front focal plane of MO obliquely and the image plane of the CMOS camera should be correspondingly located in the rear focal plane of the DL obliquely. Because the IL has a limited depth of field, this method might not be suitable for a large sample. The GRIN lens has such a small size that the consideration about the depth of field can be ignored.

5. Conclusions

Based on Fresnel's equations and full-field heterodyne interferemetry, an alternative method for measuring the full-field refractive index distribution of a GRIN lens has been proposed. Circular heterodyne light is incident on the G obliquely. The reflected light passes through the AN and the IL, and is recoded by the C. By using Chen's technique, each pixel records a group of periodic sinusoidal segments. Next, let its period τ be lengthened to $\tau + (V_\pi - V)/Vf$, then it can be modified to a continuous sinusoidal signal. The phase of the sinusoidal signal is derived with the least-squares sine-wave-fitting algorithm. If these processes are applied to other pixels, then their phases can be obtained similarly. Finally, the full-field phase distribution $\phi(x, y)$ can be obtained. The estimated data are substituted into the special equations derived from Fresnel's equations, and the two-dimensional refractive index distribution of the G can be obtained. The validity of this method has been demonstrated. This method has the merits of both common-path interferemetry and full-field heterodyne interferometry, that is, high stability, simple configuration, easy operation, time-saving and high resolution. Therefore, it possesses a great potential in clinical diagnosis of early dental caries [27], the variation of a molecular thin film or monolayers [28], the dispersive properties of optical materials [29], etc.

Acknowledgment

This study was supported in part by the National Science Council, Taiwan, Republic of China, under contract NSC95-2221-E009-236-MY3.

References

[1] Gomez-Reino C, Perez M and Bao C 2002 *Gradient-Index Optics: Fundamentals and Applications* (Berlin: Springer)
[2] Marchand E W 1978 *Gradient Index Optics* (New York, NY: Academic)
[3] Saleh B E A and Teich M C 2007 *Fundamentals of Photonics* 2nd edn (Hoboken, NJ: Wiley)
[4] Li X and Yu W 2008 Deep tissue microscopic imaging of the kidney with a gradient-index lens system *Opt. Commun.* **281** 1833–40
[5] Zickar M, Noell W, Marxer C and De Rooij N 2006 MEMS compatible micro-GRIN lenses for fiber to chip coupling of light *Opt. Express* **14** 4237–49
[6] Dragomir N M, Goh X M and Roberts A 2008 Three-dimensional refractive index reconstruction with quantitative phase tomography *Microsc. Res. Tech.* **71** 5–10
[7] Roberts A, Ampem-Lassen E, Barty A, Nugent K A, Baxter G W, Dragomir N M and Huntington S T 2002 Refractive-index profiling of optical fibers with axial symmetry by use of quantitative phase microscopy *Opt. Lett.* **27** 2061–3
[8] Chao Y F and Lee K Y 2005 Index profile of radial gradient index lens measured by imaging ellipsometric technique *Japan. J. Appl. Phys.* **44** 1111–4
[9] Bachim B L, Gaylord T K and Mettler S C 2005 Refractive-index profiling of azimuthally asymmetric optical fibers by microinterferometric optical phase tomography *Opt. Lett.* **30** 1126–8
[10] Hsieh H C, Chen Y L, Wu W T and Su D C 2009 Method for measuring the refractive index distribution of a GRIN lens with heterodyne interferometry *Proc. SPIE* **7390** 73900G
[11] Gorski W 2006 Tomographic microinterferometry of optical fibers *Opt. Eng.* **45** 125002
[12] Jones C E, Atchison D A, Meder R and Pope J M 2005 Refractive index distribution and optical properties of the isolated human lens measured using magnetic resonance imaging (MRI) *Vis. Res.* **45** 2352–66
[13] Acosta E, Flores R, Vazquez D, Rios S, Garner L and Smith G 2002 Tomographic method for measurement of the refractive index profile of optical fibre performs and rod GRIN lenses *Japan. J. Appl. Phys.* **41** 4821–4
[14] Chen Y L and Su D C 2008 Method for determining full-field absolute phases in the common-path heterodyne interferometer with an electro-optic modulator *Appl. Opt.* **47** 6518–23
[15] IEEE 2001 Standard for Terminology and Test Methods for Analog-to-Digital Converters *IEEE Std.* **1241–2000** 25–9
[16] Farrell C T and Player M A 1994 Phase-step insensitive algorithms for phase-shifting interferometry *Meas. Sci. Technol.* **5** 648–52

[17] Born M and Wolf E 1999 *Principles of Optics* 7th edn (Oxford: Pergamon) p 40
[18] Rastogi P K 1997 *Optical Measurement Techniques and Applications* (Boston, MA: Artech House) p 101
[19] Lin J Y, Chen K H and Chen J H 2007 Optical method for measuring optical rotation angle and refractive index of chiral solution *Appl. Opt.* **46** 8134–9
[20] Lee J Y and Su D C 1996 A method for measuring Brewster's angle by circularly polarized heterodyne interferomery *J. Opt.* **29** 349–53
[21] Su D C, Chiu M H and Chen C D 1996 Simple two frequency laser *Precis. Eng.* **18** 161–3
[22] Jian Z C, Chen Y L, Hsieh H C, Hsieh P J and Su D C 2004 An optimal condition for the full-field heterodyne interferometry *Opt. Eng.* **46** 115604
[23] Hou W and Wilkening G 1992 Investigation and compensation of the nonlinearity of heterodyne interferometers *Precis. Eng.* **14** 91–8
[24] De Freitas J M and Player M A 1993 Importance of rotational beam alignment in the generation of second harmonic errors in laser heterodyne interferometry *Meas. Sci. Technol.* **4** 1173–6
[25] Dou Q, Ma H, Jia G, Chen Z, Cao K and Zhang T 2007 Study on measurement of linear electro-optic coefficient of a minute irregular octahedron cBN wafer *Opt. Laser Technol.* **39** 647–51
[26] Chou C, Shyu J C, Huang Y C and Yuan C K 1998 Common-path optical heterodyne profilometer: a configuration *Appl. Opt.* **37** 4137–42
[27] Zhou M, Yao X S, Yao H, Liang Y, Liu T, Li Y, Wang G and Lan S 2009 Measurement of the refractive index of human teeth by optical coherence tomography *J. Biomed. Opt.* **14** 034010
[28] Hobley J, Oori T, Kajimoto S, Gorelik S, Hönig D, Hatanaka K and Fukumura H 2008 Laser-induced phase change in Langmuir films observed using nanosecond pump-probe Brewster angle microscopy *Appl. Phys.* A **93** 947–54
[29] Galli M, Marabelli F and Guizzetti G 2003 Direct measurement of refractive-index despersion of transparent media by white-light interferometry *Appl. Opt.* **42** 3910–4